Journal of Power Sources 188 (2009) 489–497

Contents lists available at ScienceDirect

Journal of Power Sources

journal homepage: www.elsevier.com/locate/jpowsour

Single-phase ceramics with $La_{1-x}Sr_xGa_{1-y}Mg_yO_{3-\delta}$ composition from precursors obtained by mechanosynthesis

A. Moure [a,*], A. Castro [b], J. Tartaj [a], C. Moure [a]

[a] Instituto de Cerámica y Vidrio, CSIC, C/Kelsen 5, 28049 Madrid, Spain
[b] Instituto de Ciencia de Materiales de Madrid, CSIC, c/Sor Juana Inés de la Cruz, 3 Cantoblanco, 28049 Madrid, Spain

ARTICLE INFO

Article history:
Received 25 September 2008
Received in revised form 28 October 2008
Accepted 16 November 2008
Available online 3 December 2008

Keywords:
Solid oxide fuel cell
Electrolyte
Lanthanum–gallate
Mechanosynthesis

ABSTRACT

Dense ceramics with $La_{0.80}Sr_{0.20}Ga_{0.85}Mg_{0.15}O_{2.825}$ and $La_{0.80}Sr_{0.15}Ga_{0.85}Mg_{0.20}O_{2.825}$ compositions have been prepared by sintering of mechanosynthesized precursors. The perovskite is synthesized after 85 h of milling in a planetary mill. Single phases have been obtained at conditions that are not possible if traditional solid-state reaction (SSR) method is used. The influence of milling time and composition in the reactivity of the precursors is studied. Highest purity is obtained in Sr = 0.15 and Mg = 0.20 composition, with relative density higher than 97%. The total elimination of typical secondary phases for these compositions, as $SrLaGaO_4$ and $SrLaGa_3O_7$, allows the total conductivity of the ceramics to be improved. The influence of the grain size and the nature of the grain boundaries on the electrical characteristic of the ceramics are also discussed.

1. Introduction

Ceramics with Sr- and Mg-doped $LaGaO_3$ composition with perovskite structure have received much attention in the last years as candidates for uses as electrolytes in solid oxide fuel cells working at intermediate temperatures (IT-SOFC). These are electrochemical devices that directly convert chemical energy into electrical energy and, on contrary to batteries, they work continuously consuming a fuel (generally hydrogen) of some sort [1]. The most common electrolyte material is the so-called yttrium-stabilized zirconia (YSZ), which are compositions of ZrO_2, optimized by doping with 8% mol Y_2O_3. However, this material has a limit its performance at temperatures of the order of 900–1000 °C due to its relatively low ionic conductivity (<0.1 S cm^{-1}) [2].

Ceramics with $La_{1-x}Sr_xGa_{1-y}Mg_yO_{3-\delta}$ composition presents good characteristics for uses as electrolytes in SOFC applications at intermediate temperatures (700–1000 °C). The doping of the perovkite $LaGaO_3$ with Sr (in La-sites) and Mg (in Ga sites) introduces a quantity of oxygen vacancies that results in a high conductivity (>0.10 S cm^{-1} at 800 °C). Moreover, these composition have negligible electronic conduction at temperatures T<1000 °C over a broad range of oxygen partial pressure from PO_2 = 1 to ~10^{-22} atm [3], and a stable performance over long operating times [4,5]. This results in a better performance of the cell [6]. The highest conductivity at 800 °C in ceramics with these composition have been reported to be in compositions with x = 0.20, y = 0.17, with values of 0.166 S cm^{-1} [5].

The problems related with $La_{1-x}Sr_xGa_{1-y}Mg_yO_{3-\delta}$ compositions are the appearance of secondary phases [7], mainly $Sr_3La_4O_9$, $SrLaGa_3O_7$ and $SrLaGaO_4$. They reduce the conductivity of the ceramics [8], which influences in the performance of the fuel cell. In particular, common secondary phase $SrLaGaO_4$ has poor mechanical strength due to easy cleavage fracture along a–b planes [9]. Its presence can thus facilitate the creation and propagation of cracks through the ceramics. Classical synthesis method by solid-state reaction (SSR) involves high sintering temperatures that do not fully eliminate the secondary phases and that can lead to compositional inhomogeities due to Ga evaporation [10].

Alternative synthesis routes have been tested with two aims: to reduce the final sintering temperature and to avoid the presence of secondary phases. Most of them are based on chemistry methods. Some of them have been shown to be effective to eliminate the secondary phase, although for composition with x and y values different than the ones chosen for this work (x = 0.20 and y = 0.15, with a reported conductivity of 0.149 S cm^{-1}). As examples, sol–gel [11], Pechini [12], fuel-rich glycine-nitrate synthesis [13] or organic precursor method with tartaric acid [14]. However, these chemistry-based routes have some drawbacks. They require high purity inorganic or even organometallic reactants, those are sensitive to light or humidity and are more expensive than the widely available oxides and carbonates.

Mechanosynthesis is a cleaner and economic alternative to obtain highly reactive ceramic precursors. In this method, part of the energy necessary to produce the chemical reaction is sup-

* Corresponding author.
E-mail address: alberto.moure@icv.csic.es (A. Moure).

0378-7753/$ – see front matter © 2008 Elsevier B.V. All rights reserved.
doi:10.1016/j.jpowsour.2008.11.103

plied by mechanical means. During the process, the particle size of the crystals is reduced and the homogeneity of the mixture is increased [15]. It improves the reactivity of the precursors and allows to optimise the compaction of the green pellet [16]. The processing of highly dense ceramics [17,18] is possible in a single thermal process in which grain growth and sintering take place. The power of this processing route has been recently proved. The combination of mechanochemical activation and SPS provides highly dense ceramics at sintering temperatures as low as 550–600 °C for $0.92PbZn_{1/3}Nb_{2/3}O_3$–$0.08PbTiO_3$ compositions [19].

Mechanosynthesis can produce precursors that lead to ceramics with the ideal microstructure for applications as electrolytes. That is, low porosity (lower than 5%), homogenous grain size distribution and with an adequate grain size: large enough to reduce the grain boundary density and thus the blocking effect on the conductivity [20], and small enough to preserve good mechanical properties [13]. Its application to ceramic electrolytes for SOFCs is barely found in the literature, in particular for $La_{1-x}Sr_xGa_{1-y}Mg_yO_{3-\delta}$ compositions. Gomes et al. reported [21] a reduction of the synthesis temperature of the perovskite after mechanical activation, although the presence of $LaSrGa_3O_7$ was detected by XRD. They applied it to $La_{0.95}Sr_{0.05}Ga_{0.90}Mg_{0.10}O_{3-\delta}$ composition, with a limited number of oxygen vacancies due to the small quantity of dopants Sr and Mg. This implies a limitation of the conductivity. Highly dense ceramics at relatively low sintering temperature (1450 °C for 4 h) were achieved. Zyryanov et al. obtained by mechanosynthesis powders with higher amount of dopants [22,23], with $La_{0.80}Sr_{0.15}Ga_{0.85}Mg_{0.20}O_{2.825}$ composition. However, they applied the obtained precursors to the sintering of nanocomposites with mixed ionic–electronic conductivity. The effect on sintering of single-phase LSGM ceramics was not reported.

In this work, ceramics with $La_{0.80}Sr_{0.20}Ga_{0.85}Mg_{0.15}O_{2.825}$ and $La_{0.85}Sr_{0.15}Ga_{0.80}Mg_{0.20}O_{2.825}$ compositions have been prepared by mechanosynthesis and compared with the ones obtained by classical SSR. The compositions were chosen due to their high conductivity previously reported (in the order of 0.15 S cm^{-1} [5]), and can allow to study the possibility of mechanical activation to overcome the known difficulties in obtaining single-phase ceramics when the Sr content in the composition increases. The effect of the time milling and composition on the processing of the ceramics is shown. Measurements of the conductivity by impedance spectroscopy were also carried out and related with the microstructure of the ceramics and the presence of secondary phases.

2. Experimental procedure

Ceramic precursors of $La_{0.80}Sr_{0.20}Ga_{0.85}Mg_{0.15}O_{2.825}$ and $La_{0.80}Sr_{0.15}Ga_{0.85}Mg_{0.20}O_{2.825}$ (hereinafter LSGM 20/15 and LSGM 15/20, respectively) were obtained by mechanosynthesis. The stoichiometric quantities of La_2O_3, Ga_2O_3, MgO and $SrCO_3$ necessary to obtain 4 g of the ceramic precursors were placed in a stainless-steel pot with five also stainless steel balls, 2 cm diameter, 35 g mass. Mechanochemical activation was carried out with a Pulverizette 6 model Fritsch planetary mill operating at 300 rpm. For the sake of comparison, 10 g of precursors with the same two compositions were obtained by classical SSR method (SSR precursors). Stoichiometric mixtures were calcined at final conditions of 1300 °C, 16 h, and then attrition milled during 2 h and sieved with a 100 μm sieve.

Evolution with time of the mechanochemically activated precursors was monitored by Bragg-Brentano X-ray diffraction (XRD) with a Bruker AXS D8 Advance diffractometer. Cu Kα radiation (λ = 1.5418 Å) and a 5×10^{-2} ° s^{-1} scan rate were used. Both milled and solid-state obtained precursors were treated at several temperatures, as detailed later, and characterized by XRD in a Siemens D5000 diffractometer, typically at 3.3×10^{-2} ° s^{-1} scan rate.

The crystal size (t) was obtained from the XRD data using the Scherrer formula: $t = 0.9\lambda/B\cos\theta_B$, where λ is the wavelength used, B is the full width at half maximum of the diffraction peak and θ_B is the Bragg angle [24]. BET surface area of the calcined powder was measured using a Quantachrome Accusorb instrument.

Initial oxides and carbonates mixture and the ones after prolonged milling were studied by differential thermal analysis (DTA)–thermogravimetric (TG) techniques. For the first one, a thermoanalyzer Netzsch, model STA-409 was used up to 1200 °C, in an alumina crucible with a heating rate of 5 °C min^{-1}. For the second one, the same thermoanalyzer was used up to 1500 °C, in a Pt crucible, and with a heating rate of 10 °C min^{-1}.

Between 0.7 and 1 g of the powders were uniaxially pressed in pellets with 0.8 mm diameter at 100 MPa and then isostatically pressed at 200 MPa. The shrinkage behaviour was studied using a dilatometer Netzsch Gerätebau (model 402 EP, Selb-Bayern Germany) up to 1550 °C with a heating and cooling rate of 5 °C min^{-1}.

The pellets were then sintered in air at conditions detailed later and based on the dilatometric results, and then characterized by XRD at the same conditions as for the precursors. Density of the ceramics was measured by Archimede's method in distilled water at room temperature. After polishing and thermal etching, the microstructures of the sintered samples were examined by scanning electron microscopy in a Zeiss Microscope (model DSM 950, Oberkochem, Germany). Impedance was measured using a LF Impedance analyzer (model HP-4294A, Hewlett-Packard) on disk pellets with electrodes of Ag (Dupont) calcined at 700 °C, 1 h.

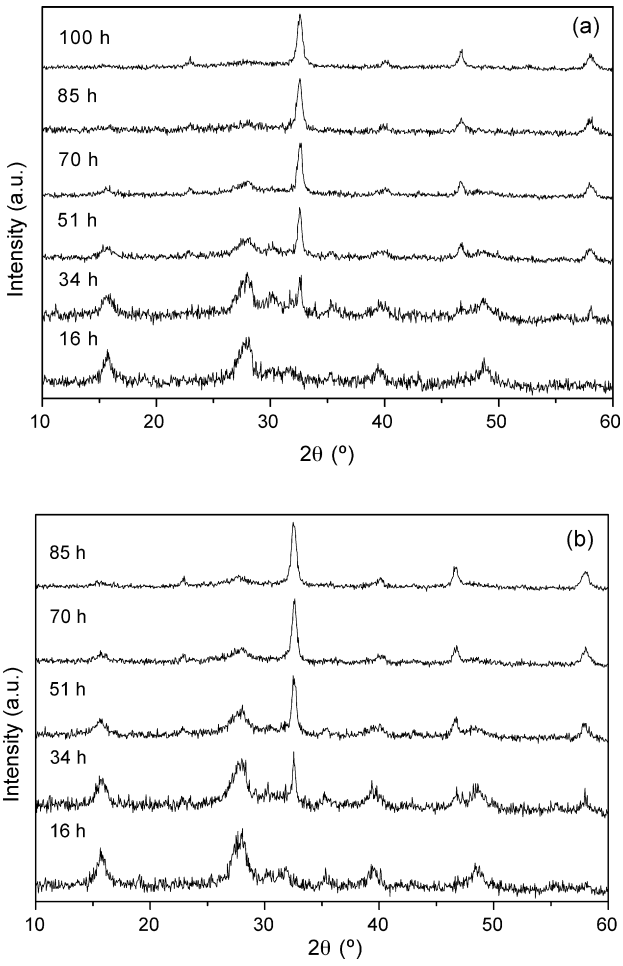

Fig. 1. XRD patterns of the stoichiometric mixture of La_2O_3, MgO, $SrCO_3$, Ga_2O_3, precursor of: (a) $La_{0.80}Sr_{0.20}Ga_{0.85}Mg_{0.15}O_{2.825}$ and (b) $La_{0.85}Sr_{0.15}Ga_{0.80}Mg_{0.20}O_{2.825}$ ceramics, after different milling times.

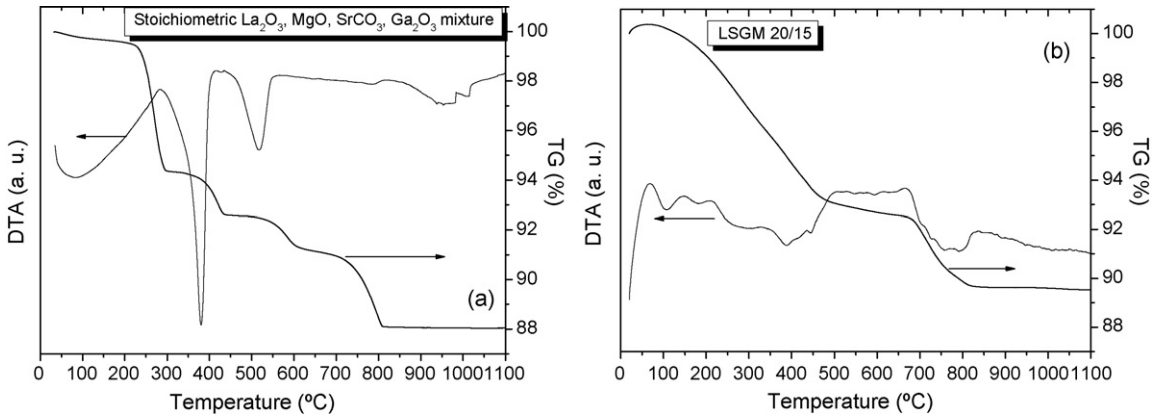

Fig. 2. DTA and TG curves of a mixture of 0.4 La_2O_3, 0.15 MgO, 0.2 $SrCO_3$, and 0.425 Ga_2O_3: (a) without milling and (b) after 85 h of milling.

3. Results

Fig. 1 shows the evolution with time of the oxides and carbonate mixture for LSGM 20/15 milled up to 85 and 100 h, and for LSGM 15/20 milled up to 85 h. In all cases, the peaks that can be indexed as corresponding to the perovskite phase begin to appear after about 35 h of milling. After 85 h, the diffraction corresponds to the perovskite structure together with an amorphous to XRD halo. An increasing of the milling time to 100 h does not change the appearance of the diffraction pattern, although the characteristics of the precursors are different, as it will be explained later.

Fig. 2 shows the DTA–TG curves of the mixture of the composition LSGM 20/15 after milling during 85 h. It is compared with the initial mixture of oxides and carbonates to obtain precursors of ceramics with the same composition. For this latter, weight loss is observed in four steps, corresponding to four endothermic peaks in the DTA curves. The last two ones are related with two wide

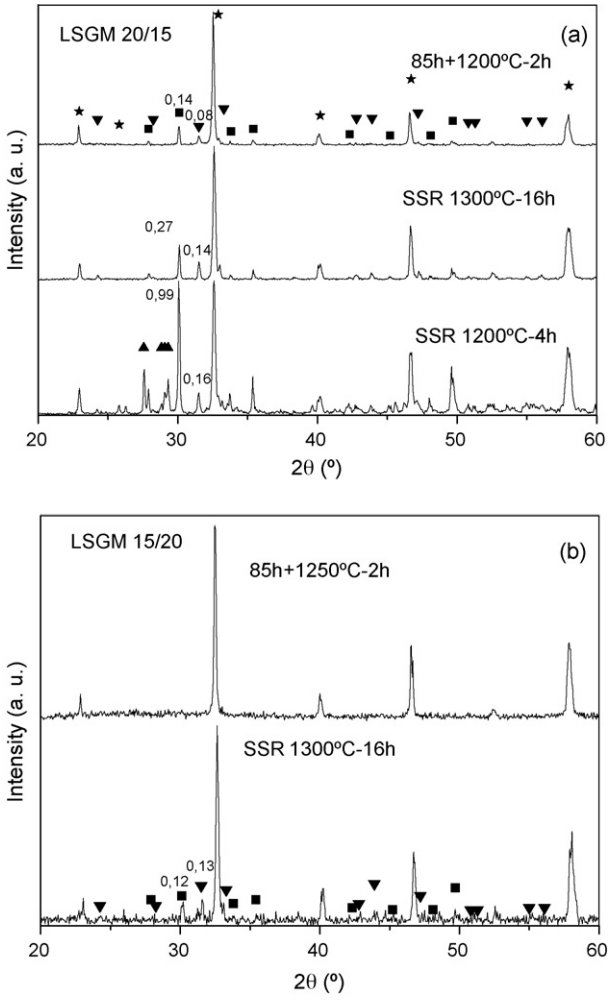

Fig. 3. XRD patterns after thermal treatment of: (a) $La_{0.80}Sr_{0.20}Ga_{0.85}Mg_{0.15}O_{2.825}$ precursors prepared by solid-state reaction and mechanical activation after 85 h of milling and (b) same for $La_{0.85}Sr_{0.15}Ga_{0.80}Mg_{0.20}O_{2.825}$ composition (*, perovskite; ■, $SrLaGa_3O_7$; ▼, $SrLaGaO_4$; ▲, $Sr_3La_4O_9$).

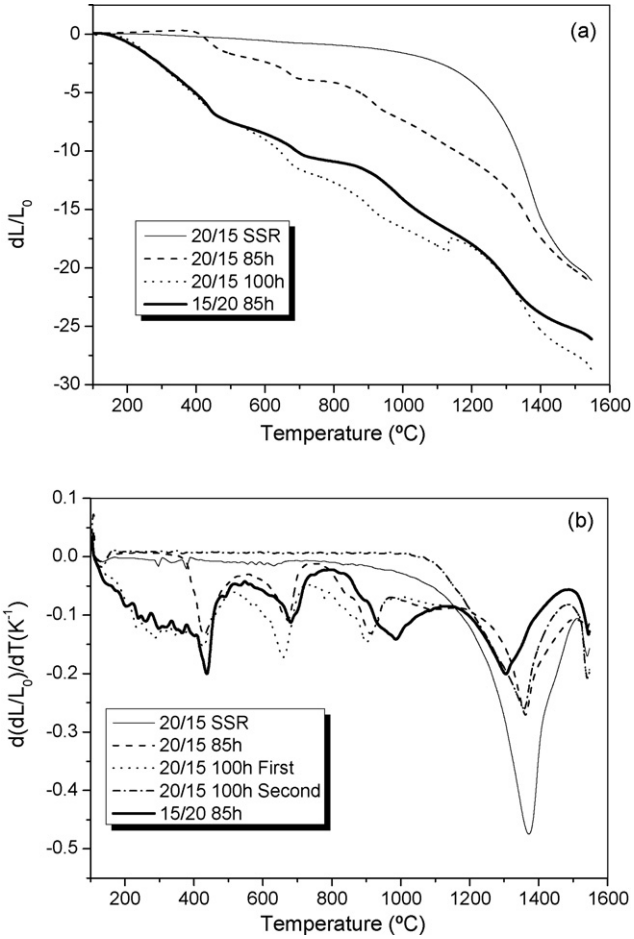

Fig. 4. (a) Shrinkage and (b) shrinkage rate of green pellets of $La_{0.80}Sr_{0.20}Ga_{0.85}Mg_{0.15}O_{2.825}$ and $La_{0.85}Sr_{0.15}Ga_{0.80}Mg_{0.20}O_{2.825}$ compositions.

endothermic peaks. For the milled sample, the first three defined steps are now a continuous weight loss, while the fourth step also appears between 700 and 800 °C. The wide endothermic peak (composed by two smaller peaks) between 800 and 1100 °C for the mixture without mechanical treatment appears in the milled sample between 700 and 900 °C.

Fig. 3 shows XRD patterns of the LSGM 20/15 composition after different thermal treatment of the precursor obtained by classical SSR and after milling during 85 h, respectively, for LSGM 20/15 and 15/20 compositions. At reduced temperature (1200 °C, 4 h), three secondary phases with $Sr_3La_4O_9$, $SrLaGa_3O_7$ and $SrLaGaO_4$ composition are detected besides the ones corresponding to the perovskite phase for SSR precursors. The number expresses the relative intensity of the most intense peaks of each phase with regard to the perovskite one. The increase of the calcination temperature eliminates $Sr_3La_4O_9$ phase, but the $SrLaGa_3O_7$ and $SrLaGaO_4$ ones appear even at 1300 °C, 16 h. These latter phases also appear for the mechanosynthesized powder, although the relative intensity is clearly lower at reduced processing temperatures (1200 °C, 2 h). For LSGM 15/20 composition, $SrLaGa_3O_7$ and $SrLaGaO_4$ appear at 1300 °C, 16 h for the SSR precursors. However, calcination at 1250 °C, 2 h of the mechanosynthesized precursors leads to single perovskite XRD patterns.

Fig. 4 shows the shrinkage studies of green pellets prepared from classical SSR and for mechanosynthesized precursors at different conditions and for the two compositions. Fig. 4a shows the shrinkage of the pellets and Fig. 4b shows the shrinkage rates. The curve corresponding to LSGM 20/15 after 100 h milling is composed of a first measurement up to 1130 °C, then cooling to room temperature and re-heated up to 1550 °C (due to a experimental error). The shrinkage of the sample with SSR precursors has a unique step, beginning at 1000 °C, approximately, with a maximum shrinkage rate located at 1370 °C. For the activated precursors, there are three steps prior to the maximum shrinkage. For the 20/15 composition, the maximum rate fits with the one of the SSR, while for the 15/20 composition it is located at 1300 °C, approximately.

Table 1
Density measured by Archimede's method of $La_{0.80}Sr_{0.20}Ga_{0.85}Mg_{0.15}O_{2.825}$ and $La_{0.85}Sr_{0.15}Ga_{0.80}Mg_{0.20}O_{2.825}$ ceramics.

Solid-state synthesis	1400 °C, 12 h	1450 °C, 12 h	1500 °C, 6 h
LSGM 20/15 (1300 °C, 16 h)	96.2%*	99.6%*	96.6%*
Mechanosynthesis	**1320 °C, 12 h**	**1380 °C, 12 h**	**1430 °C, 12 h**
LSGM 20/15 (85 h)	No	No	96.1%*
LSGM 20/15 (100 h)	94.8%*	95.2%	95.5%
LSGM 15/20 (85 h)	97.0%	98.1%	97.9%

Asterisks denote the ceramics where secondary phases were observed by XRD.

The aspect of the shrinkage curve led to different sintering strategies for activated precursors and the ones obtained by SSR. For the former, two intermediate plateaus at 400 and 800 °C during 1 h were carried out during the heating. For the latter, heating to the sintering temperature was carried out in only one step. Fig. 5 shows the XRD patterns of the ceramics obtained from SSR and activated precursors, respectively. For SSR precursors, even at the highest sintering temperatures (1500 °C, 6 h), peaks corresponding to $SrLaGa_3O_7$ secondary phase appear. Its presence diminishes as sintering temperature increases.

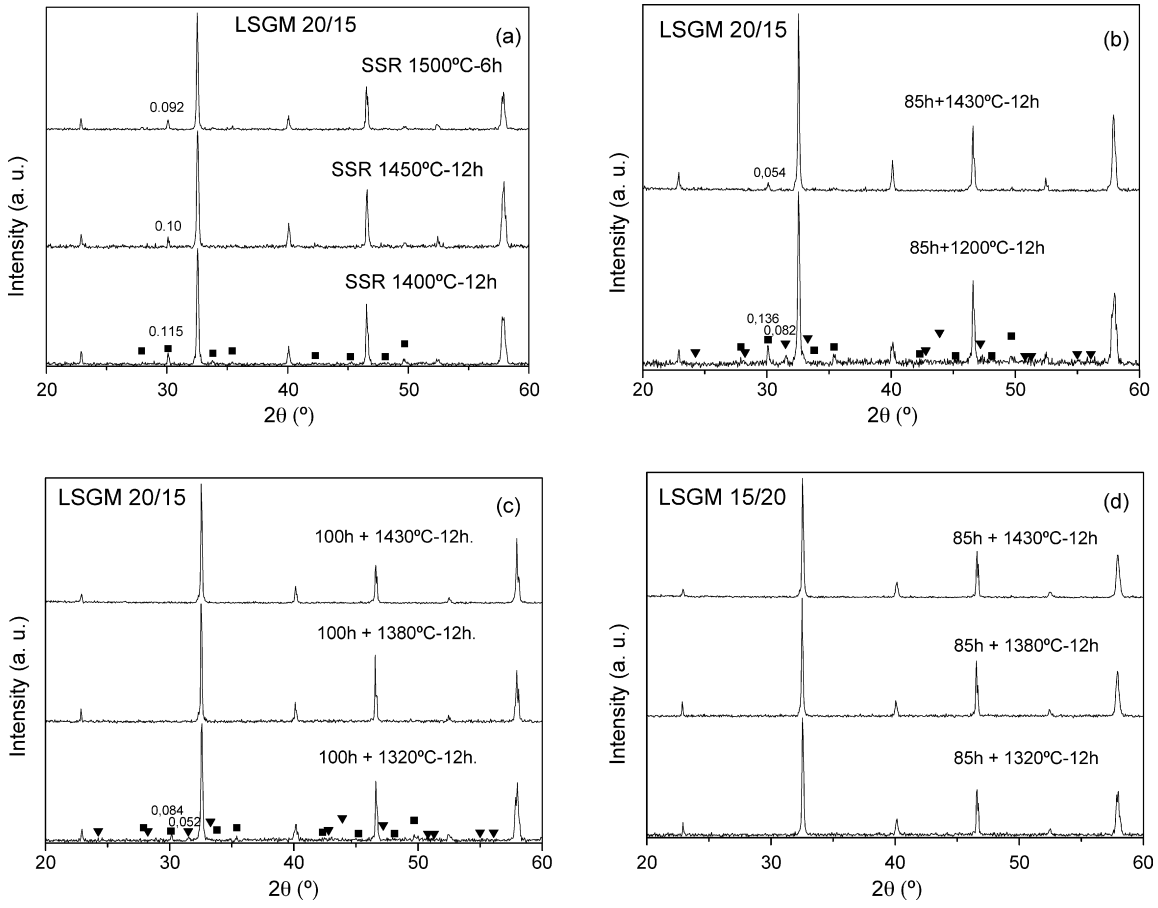

Fig. 5. XRD patterns of $La_{0.80}Sr_{0.20}Ga_{0.85}Mg_{0.15}O_{2.825}$ ceramics sintered from precursors obtained by (a) SSR; and precursors obtained by mechanosynthesis after (b) 85 h and (c) 100 h of milling and (d) $La_{0.85}Sr_{0.15}Ga_{0.80}Mg_{0.20}O_{2.825}$ composition from precursors obtained by mechanosynthesis after 85 h of milling.

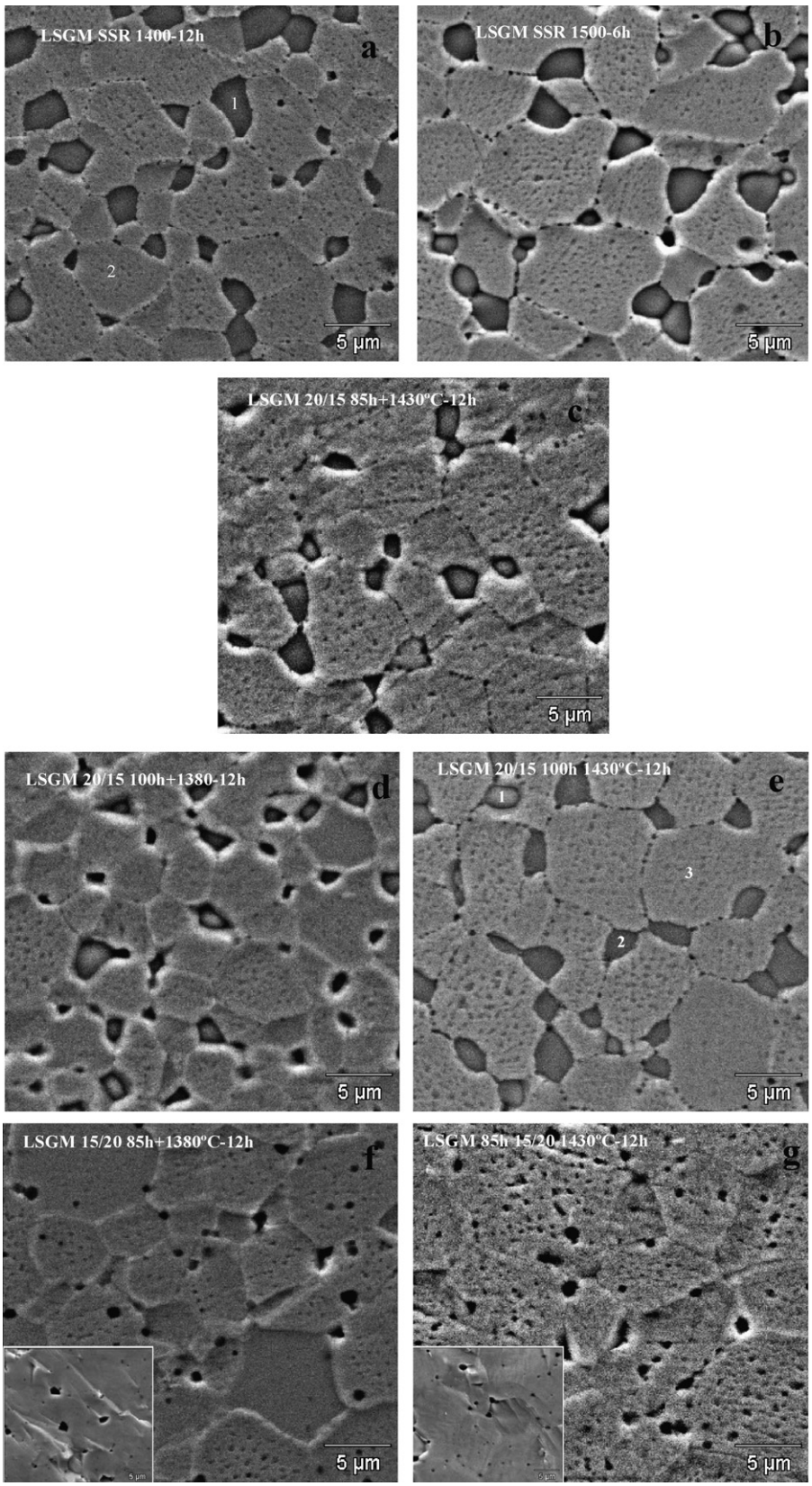

Fig. 6. SEM micrographs of ceramics: $La_{0.80}Sr_{0.20}Ga_{0.85}Mg_{0.15}O_{2.825}$ composition from SSR precursors sintered at: (a) 1400 °C, 12 h, (b) 1500 °C, 6 h, from activated precursors milled up to (c) 85 h, 1430 °C, 12 h, (d) 100 h, 1380 °C, 12 h, and (e) 100 h, 1430 °C, 12 h; and $La_{0.85}Sr_{0.15}Ga_{0.80}Mg_{0.20}O_{2.825}$ composition from activated precursors milled up to (f) 85 h, 1380 °C, 12 h and (g) 1430 °C, 12 h.

For the mechanosynthesized precursors, differences are found for different milling times and composition. For the LSGM 20/15 composition milled during 85 h, traces of $SrLaGa_3O_7$ secondary phase are detected at the highest sintering temperature (1430 °C, 12 h). However, the increase of the milling time to 100 h makes the ceramics to be single phase to XRD after sintering at 1380 °C. The situation is improved for the LSGM 15/20 composition. Even at the lowest sintering temperature (1320 °C, 12 h) ceramics are single phase.

Table 1 shows the densities of the sintered ceramics measured by Archimedes's method. The theoretical density has been calculated from the division of the molecular weight by the cell volume calculated by Datta et al. [25], giving place to a value of 6.68 g cm^{-3} for LSGM 20/15 composition and 6.67 g cm^{-3} for LSGM 15/20. The asterisks mark the ceramics where secondary phases have been detected by XRD. Thus, the density measured for those ceramics has a certain error, which cannot be exactly determined. Some trends can be observed. Relative density at optimized conditions (maximum density) is higher for ceramics from SSR precursors and within activated precursors, for LSGM 15/20 composition, for which the sintering at 1320 °C (slightly higher than the temperature of maximum shrinkage) produces single-phase ceramics with 97% of density.

Fig. 6 shows the micrographs of polished thermally etched ceramics sintered from SSR, and mechanosynthesized precursors after 85 and 100 h of milling, for LSGM 20/15 and LSGM 15/20 compositions. Different sintering conditions are also compared. Two phases (one darker within a clearer matrix) are easily distinguished for the ceramics sintered from SSR precursors (Fig. 6a and b), and for the mechanically treated during 85 h (1430 °C, Fig. 6c) and 100 h (1380 °C, Fig. 6d and 1430 °C, Fig. 6e, where a third phase marked with a "3" is also observed) in the LSGM 20/15 compositions. The amount of secondary phase seems to diminish for the ceramics from mechanosynthesized powders. It is remarkable that secondary phases not detected by XRD (Fig. 5c) appear now in the SEM images (Fig. 6d and e). An increase in the sintering temperature affects only slightly to the size of secondary phases. For the LSGM 15/20 activated composition (Fig. 6f and g), only the clearest matrix phase appears without secondary phases. EDS analysis was carried out on the different phases observed in the micrographs, marked as 1, 2 and 3 in Fig. 6a and e. Results are shown in Table 2. From the images, it is also observed that if similar processing conditions are compared (85 h activation, 1430 °C sintering temperature), grain size is higher for Mg-rich (LSGM 15/20) compositions. Fig. 6f and g have an inset where transgranular fracture micrographs are shown. They proved that the appearance of a higher porosity in LSGM 15/20 composition ceramics is in fact due to pull-out during polishing. Polished surfaces micrographs are shown for a better comparison of the grain size.

Fig. 7 shows the impedance spectra at approximately 300 °C of the LSGM ceramics, as representative of the observed at different temperatures. The arcs at higher conductivity are associated with the bulk conductivity and the ones at intermediate frequencies with grain boundary conductivity. The tails observed at lower frequencies are associated to the interface ceramic–electrode.

Table 2
EDS analysis (wt.%) of matrix and secondary phases marked in points shown in Fig. 6a and e.

	O–K	Ga–K	Sr–L	La–L
LSGM 15/20 SSR 1400 °C, 12 h				
Point 1	21.70	47.48	2.72	28.10
Point 2	19.10	29.85	0.89	50.15
LSGM 20/15 100 h 1430 °C, 12 h				
Point 1	20.54	39.59	1.97	37.91
Point 2	21.31	44.84	2.41	31.45
Point 3	19.23	30.70	0.90	49.17

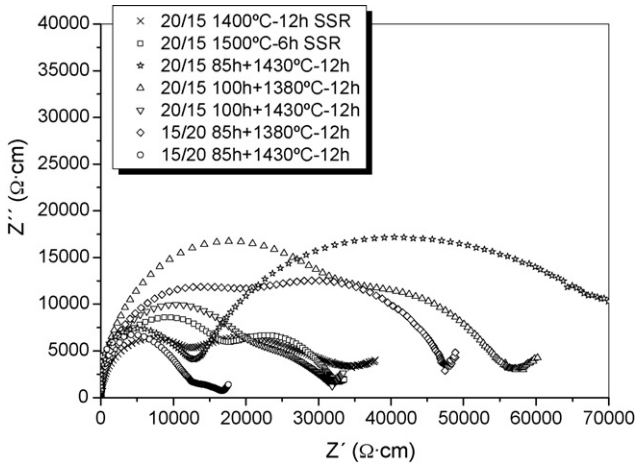

Fig. 7. Impedance spectra of ceramics with $La_{1-x}Sr_xGa_{1-y}Mg_yO_{3-\delta}$ composition at temperatures close to 300 °C.

Fig. 8 shows the Arrhenius plots of the bulk, grain boundary and total conductivity for ceramics obtained from SSR and mechanosynthesized precursors, obtained from impedance spectra similar to the ones shown in Fig. 7. Those sintered at higher temperatures (1430 and 1500 °C) present the highest total conductivity, and within them, the ones prepared from precursors mechanosynthesized during 100 h (LSGM 20/15) and 85 h (LSGM 15/20) have higher conductivity. Although no so clearly marked, this trend is also observed for both bulk and grain boundary conductivity. Table 3 shows the activation energy values at the different processing conditions obtained from the slope of the Arrhenius plot.

4. Discussion

As Fig. 1 shows, powders with perovskite structure can be obtained by mechanosynthesis of the mixture of oxides and carbonate. Crystal sizes obtained from the XRD data by using the Scherrer equation are 25 and 30 nm for these powdered perovskites with LSGM 20/15 and 15/20, respectively. The values of specific surface area were found to be 30.5 and 25.5 m^2 g^{-1}, respectively. Taken the relation between particle size (D) and specific surface (S) given by $D = 6/d_{th} \times S$, where d_{th} is the theoretical density, calculated crystallites sizes are 30 and 35 nm. This result confirms the ones obtained by XRD results within experimental error. However, the results of the DTA and XRD of the subsequent thermal treatments show that in fact the powder obtained does not only contain perovskite phases.

DTA shows that the well-defined endothermic peaks in SSR precursors associated with weight loss up to 600 °C, approximately, are not so defined in activated precursors. Moreover, the weight loss is continuous and not in steps. Marques et al. reported [26] that at room atmosphere, La_2O_3 contains $La(OH)_3$, and that the mixture La_2O_3–$SrCO_3$ decomposes in four stages: (a) elimination of absorbed water; (b) dehydration by loss of two molecules of water; (c) dehydration by loss of two molecules of water; (d) decomposition of $SrCO_3$ with liberation of CO_2. This corresponds to the observed in the SSR powder. The weight loss occurs in the same range of temperatures for the mechanosynthesized precursors. It is due to the water absorbed in the mixture during milling and to the one incorporated on the initial oxide, with different crystallization state and size that modified the conditions where water is released. That is the reason for which the weight loss is produced in a continuous form. The total weight loss is lower for the mechanosynthesized precursor than for the SSR one, because a part of the initial La oxide

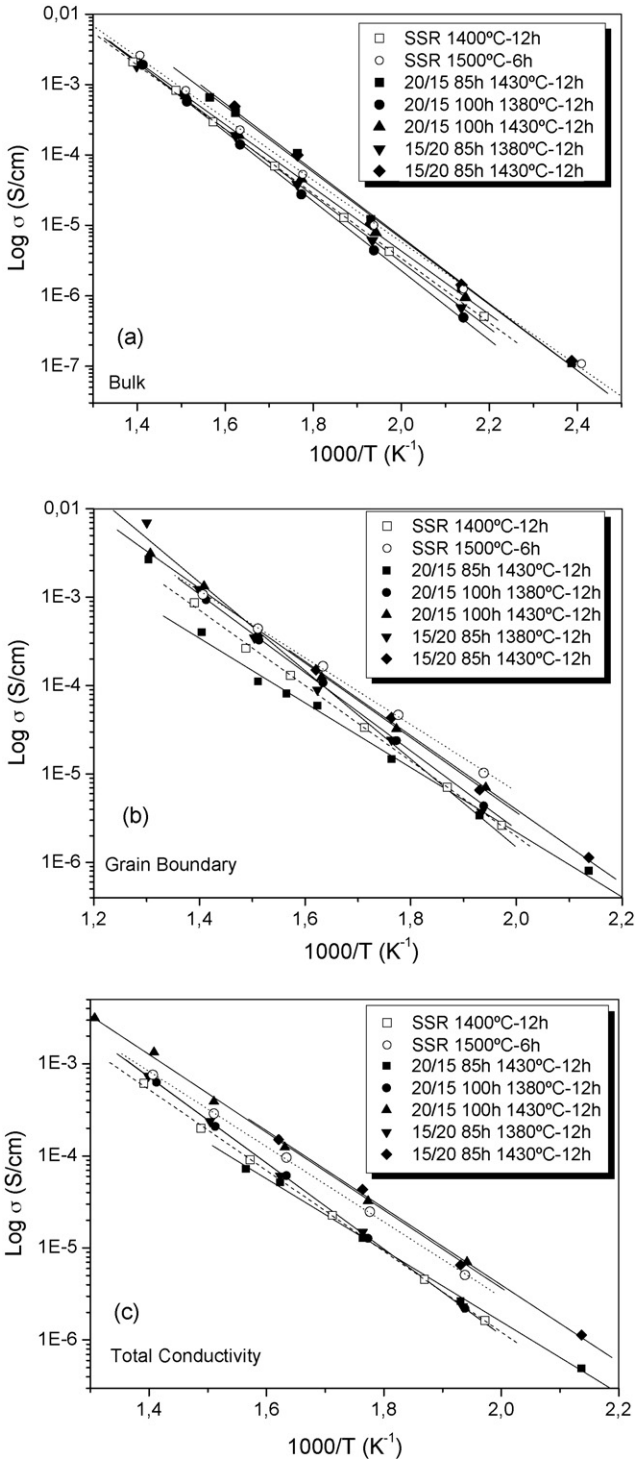

Fig. 8. Arrhenius plots of the (a) bulk, (b) grain boundary and (c) total conductivity of $La_{0.80}Sr_{0.20}Ga_{0.85}Mg_{0.15}O_{2.825}$, and $La_{0.85}Sr_{0.15}Ga_{0.80}Mg_{0.20}O_{2.825}$ ceramics.

has reacted to form the perovskite. Less amount of water can thus be trapped.

The DTA curve also presents a wide endothermic peak, composed by two smaller peaks at lower temperature for the mechanosynthesized precursor. The one at the highest temperature can be attributed to the formation of perovskite, as XRD in Fig. 3 confirms. It is produced together with intermediate phases that also appear in Fig. 3 ($Sr_3La_4O_9$, $SrLaGaO_4$ and $SrLaGa_3O_7$). Within them, $SrLaGa_3O_7$ is the most stable, and it cannot be eliminated even at the highest sintering temperature (1500 °C) for the SSR precursors. The temperature of the formation of these phases is reduced by ~300 °C by mechanosynthesis, as it is pointed out in Figs. 2 and 3. The reduction of the processing temperature after mechanical treatment is a widely observed phenomenon in the ceramics processing [16,17]. As a consequence, secondary phases appear in a lesser amount by heating mechanical activated precursors. However, for the LSGM 20/15 composition activated during 85 h, it is not possible to have single-phase ceramics according to XRD, as the peaks corresponding to $SrLaGa_3O_7$ appears even after sintering at 1430 °C, 12 h. This confirms that part of the activated powder is an amorphous rest of the initial oxides and carbonate, which react after heating and form the secondary phases. It does not disappear after later thermal treatment.

The increase of the milling time to 100 h makes the mixture to be more reactive, and single-phase ceramics according to XRD are achieved now by sintering at 1380 °C (Fig. 5). The possible drawback comes from contamination at extended milling. The milling media used in this work was stainless-steel. The mean contamination will thus come from Fe. For the powder activated during 85 h, X-ray fluorescence technique gave an estimation of ~1% in weight of Fe contamination. It must be slightly increased at longer milling times. However, this issue is not a critical factor for the compositions studied in this work. It has been reported that Fe [27–29], with an atomic radius (for Fe^{3+} is 64 pm) closer to the Ga one (Ga^{3+}, 62 pm), incorporates to the perovskite structure $La_{1-x}Sr_xGa_{1-y}Mg_yO_{3-\delta}$ composition for Fe amounts higher than 1.5 wt.%. It can even improve the ionic conductivity in $La_{0.8}Sr_{0.2}Ga_{0.8}Mg_{0.17}Fe_{0.03}O_{3-\delta}$ composition (1 wt.%) [29].

The secondary phases can be identified in the SEM images. The darkest grains marked as "1" in Fig. 6a and "2" in Fig. 6e corresponds to a Ga-rich phase as shown in EDS analysis (Table 1), and it is related with the $LaSrGa_3O_7$ phase. The clearer one indicated as "1" in Fig. 6e is associated with the $LaSrGaO_4$ composition. The results and the aspect of the phases in the micrograph are in agreement with the observed by Lu et al. [8]. Finally, the one marked as "2" in Fig. 6a and "3" in Fig. 6e as similar compositions, and are identified as the matrix perovskite phase.

It is remarkable that single-phase ceramics according to XRD show secondary phases in the SEM micrographs. These are large enough and are present in amount detectable by XRD techniques. The samples for microscopy were prepared after being lapped for conductivity measurements. Thus, surfaces of the ceramics were removed. Fig. 9 shows the XRD pattern of the LSGM 20/15 composition sintered at 1380 °C from precursors milled during 100 h (Fig. 6d) after surface removal. Peaks corresponding to the $LaSrGa_3O_7$ and $LaSrGaO_4$ phases clearly appear now. The observation of single-phase surfaces with perovskite structure and secondary phases in the bulk is a phenomenon previously observed within these compositions by Djurado and Labeau [7]. Most of the works in the literature often ignores this point, perhaps because the usual situation is the contrary, that is, surfaces with secondary phases and purer bulks. However, it must be taken into account. Even an improvement of the reactivity of the precursors by mechanosynthesis (proved by comparing the samples with the classical SSR) can lead to this situation.

A lower milling time and sintering temperature are needed for LSGM 15/20 composition to obtain pure single-phase ceramics in surface and bulk, as XRD and SEM images show. Powder treated at 1250 °C after milling of 85 h has no traces of secondary phases, while SSR powder after heating at 1300 °C, 16 h still present $SrLaGaO_4$ and $SrLaGa_3O_7$ secondary phases. Even at the lowest sintering temperatures (1320 °C, 12 h), single-phase ceramics from activated precursors are obtained, with relatively high density (97%, Table 1). It has been shown that the solubility of Sr in the structure is enhanced by adding Mg simultaneously [30]. The $LaGaO_3$ lattice is easily expanded by the addition of Mg ions, increasing the solubil-

Table 3
Activation energy for conductivity obtained from Arrhenius plots of $La_{1-x}Sr_xGa_{1-y}Mg_yO_{3-\delta}$ ceramics.

	Ceramics	E_a (bulk, eV)	E_a (grain boundary, eV)	E_a (total, eV)
Mechanosynthesis				
20/15	85 h+ 1430 °C, 12 h	0.975	0.774	0.818
20/15	100 h+ 1380 °C, 12 h	0.980	0.930	0.980
20/15	100 h+ 1430 °C, 12 h	0.940	0.891	0.912
15/20	85 h+ 1380 °C, 12h	0.984	0.974	0.979
15/20	85h+ 1430 °C, 12 h	0.979	0.951	0.965
Solid-state				
20/15	1400 °C, 12 h	0.957	0.897	0.923
20/15	1500 °C, 6 h	0.912	0.799	0.863

ity of Sr. The mechanical treatment produces a continuous mixing at atomic levels of the constituents, improving the co-doping of the perovskite structure. It favors the incorporation of Sr in the perovskite and limits the appearance of Sr-rich secondary phases, as $SrLaGaO_4$ and $SrLaGa_3O_7$.

These results implies that mechanochemical process changes somehow the phase diagram of the system La_2O_3–MgO–Ga_2O_3–SrO reported by Rozumek et al. [31] that established the solubility limit of both Sr and Mg dopants to 5 at.% each at 1250 °C. This phase diagram only considers composition and temperature, but mechanochemical process introduces a pressure-like component in the diagram. It has been shown [32] that mechanosynthesis can stabilize perovskite-structure ceramics with low tolerance factor that can be only achieved by pressure assisted. Prolonged milling introduces high level of disorder and defects that produce high crystalline strain with a compressive hydrostatic-like component, and that is retained after sintering. For LSGM 15/20 composition, the change with respect to the solid-state reacted phase diagram is evident. For LSGM 20/15 it is observed that increase of milling time to 100 h also change the phase diagram somehow, with the disappearance of secondary phases at 1380 °C, at least at the surface of the ceramic, if compared with classical SSR precursors or the ones milled during 85 h. It is consistent with the fact that strain is accumulative at longer milling time. In this case, the increase of time activation is equivalent to a higher pressure component [32] that produces a further change of phase diagram. This is a promising result, as it suggests that mechanosynthesis is a good route to prepare LSGM ceramics with higher amounts of Sr and Mg, that is, a larger number of oxygen vacancies to improve the conductivity of the electrolytes.

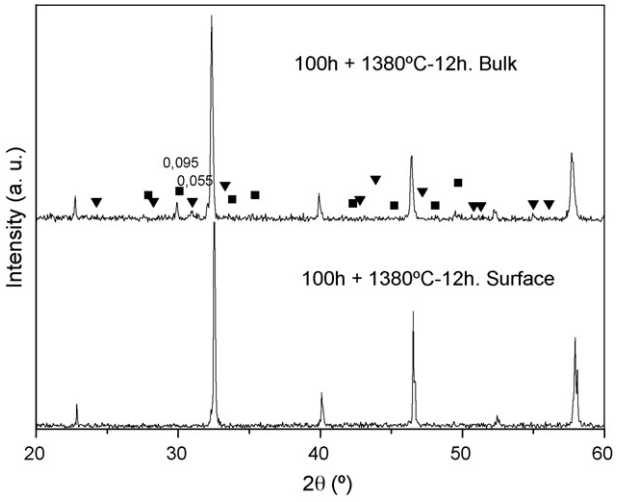

Fig. 9. XRD patterns of ceramics: $La_{0.80}Sr_{0.20}Ga_{0.85}Mg_{0.15}O_{2.825}$ composition sintered at 1380 °C, 12 h from precursors obtained by mechanical treatment up to 100 h of milling before and after surface removal.

Comparing the values of relative density of the single-phase ceramics for LSGM 20/15 and LSGM 15/20 in Table 1, the increase of Mg content favors the densification of the ceramics, but the microstructure shows that porosity is similar for both compositions. The error in measured density comes from the presence of the secondary phase in the Sr-rich ceramics. This is in agreement with that reported by Datta et al. [33]. It is remarkable the high density achieved at relatively low temperature (97 and 98% at 1320 and 1380 °C, respectively for LSGM 15/20), which is comparable with the recently reported by Oncel et al. [14] and Isikawa et al. [34] for single-phase ceramics processed by regenerative sol–gel and self-propagating high temperature synthesis, respectively.

The grain size is lower for Sr-rich composition (Fig. 6). It seems to be a consequence of the presence of secondary phases for the LSGM 20/15. It can be observed that an increase of temperature from 1400 to 1500 °C does not change greatly neither the size of the secondary phase or the matrix ones. A stable structure is achieved at early stages of the sintering, pining the perovskite phase grain boundaries. The decrease in grain growth rate probably promotes also the development of microstructure with a low porosity. On the contrary, for the LSGM 15/20 composition, no secondary phases are pinning the grain boundaries, and thus grain size can be larger at lower sintering temperatures, even at expense of the appearance of slightly larger pores.

It is worth noting that the ceramics without secondary phases has the highest total conductivity, as Fig. 8 shows. The presence of $LaSrGa_3O_7$ or $SrLaGaO_4$ phases has two effects on the conductivity. The first is an intrinsic reduction of the conductivity due to the isolating character of this phase, that at 800 °C can be three orders of magnitude lower than the perovskite one [9] for the $SrLaGaO_4$ phase. On the other hand, its appearance produce changes in the real stoichiometric of the main perovskite phase, as part of the Sr is not incorporated to the structure. It diminishes the number of oxygen vacancies and thus the conductivity.

As expected, the grain boundary conductivity is lower than the bulk one. The fact that the single-phase ceramic have higher grain boundary conductivity can be also indicative that at least part of the secondary phases segregate to the grain boundary. Their values are comparable to the ones obtained with the non-single-phase ceramic sintered form SSR precursors at 1500 °C, 6 h. It shows the importance of eliminating the secondary phases in these compositions, as well as optimizing the processing to optimize the microstructure to assure simultaneously good electrical and mechanical properties.

Due to experimental limitations, it was not possible to carry out measurements at temperatures higher than 500 °C. Moreover, it is not possible to extrapolate data from Arrhenius plots at temperatures higher than 600 °C, where these structures suffer a phase transition that results in a change in the slope of the conductivity [5,8]. The activation energies (depending on the slope of the Arrhenius plot), shown in Table 3, are similar to the reported by Huang et al. [5]. Thus, extrapolation of conductivity values from the Arrhenius plots up to 600 °C for comparing the results is possible. It

shows values of conductivity close to the reported previously at that temperature, in the range of 0.015–0.017 S cm^{-1}. The slightly lower values are attributed to different nature of grain boundary, as well as to differences in grain boundary density per volume. The similar activation energy also proves that the conductivity measured is basically ionic, due to the presence of oxygen vacancies [5].

5. Conclusions

Influence of the mechanical treatment in the processing of ceramics with $La_{0.80}Sr_{0.20}Ga_{0.85}Mg_{0.15}O_{2.825}$ and $La_{0.80}Sr_{0.15}Ga_{0.85}Mg_{0.2}O_{2.825}$ compositions have been studied. The mechanosynthesis of the perovskite is achieved after 85 h of milling.

The formation of single-phase perovskite, according to XRD analysis, is possible at lower temperatures than the needed by classical solid sate reaction when milling time or Mg content is increased. The solubility at lower temperatures of the Sr and Mg dopants in the perovskite phase is increased by effect of the prolonged milling.

For Sr = 0.20 and Mg = 0.15 composition, there are differences between surface and bulk composition, with secondary phases appearing in the core of the ceramics and disappearing at the surface. For Sr = 0.15 and Mg = 0.20, ceramics are real single phase.

Highly dense, single-phase ceramics are obtained by sintering of the mechanosynthesized precursors (98% for Mg = 0.20) at relatively lower temperatures (1380 °C, 12 h) than the needed if traditional methods are used (>1450 °C).

The conductivity of the ceramics increases when purity of the phases increases, and decreases when increasing the amount of secondary phases or the grain boundary density per volume.

Mechanosynthesis have thus shown to be a successful route to obtain dense and single-phase ceramics at relatively low temperatures with a high amount of dopants necessaries to increase the conductivity of lanthanum–gallium perovskites for applications as electrolytes in solid oxide fuel cells.

The processing route is shown to be appropriated to obtain bulk and most likely thick film ceramics of these materials with high ionic conductivity. Due to the relative low particle size obtained and low processing material temperature, the application for fabrication of thin films by adequate rheological control is also expected to be produced. Further studies are needed for the processing of thin films with these compositions.

Acknowledgments

This work was supported by Spain PROFIT CIT-120000-2007-50 and MICINN MAT2008-06785-C02-02-E. Dr A. Castro acknowledges the financial support of the Spanish MICINN (project MAT2007-61884). Dr. A. Moure is indebted to the CSIC (MICINN) of Spain for the "Junta de Ampliación de Estudios" contract (Ref JAEDOC087). The authors are grateful for the technical support provided by Ms I Martínez (ICMM).

References

[1] G. Hoogers, in: G. Hoogers (Ed.), Fuel Cell Technology Handbook, CRC Press, Boca Raton, FL, 2003, I-1–I-5.
[2] E.C. Subbarao, H.S. Maiti, Solid State Ionics 11 (4) (1984) 317–338.
[3] T. Ishihara, H. Matsuda, Y. Takita, J. Am. Chem. Soc. 116 (9) (1994) 3801–3803.
[4] P.N. Huang, A. Petric, J. Electrochem. Soc. 143 (5) (1996) 1644–1648.
[5] K.Q. Huang, R.S. Tichy, J.B. Goodenough, J. Am. Ceram. Soc. 81 (10) (1998) 2565–2575.
[6] K.Q. Huang, R. Tichy, J.B. Goodenough, J. Am. Ceram. Soc. 81 (10) (1998) 2581–2585.
[7] E. Djurado, M. Labeau, J. Eur. Ceram. Soc. 18 (10) (1998) 1397–1404.
[8] X.C. Lu, J.H. Zhu, J. Electrochem. Soc. 155 (5) (2008) B494–B503.
[9] M. Rozumek, R. Majewski, F. Aldinger, K. Kunstler, G. Tomandl, CFI-Ceram. Forum Int. 80 (4) (2003) E35–E40.
[10] W. Kuncewicz-Kupczyk, D. Kobertz, M. Miller, L. Singheiser, K. Hilpert, J. Electrochem. Soc. 148 (6) (2001) E276–E281.
[11] K.Q. Huang, M. Feng, J.B. Goodenough, J. Am. Ceram. Soc. 79 (4) (1996) 1100–1104.
[12] K.Q. Huang, J.B. Goodenough, J. Solid State Chem. 136 (2) (1998) 274–283.
[13] J.W. Stevenson, T.R. Armstrong, L.R. Pederson, J. Li, C.A. Lewinsohn, S. Baskaran, Solid State Ionics 115 (1998) 571–583.
[14] C. Oncel, B. Ozkaya, M.A. Gulgun, J. Eur. Ceram. Soc. 27 (2–3) (2007) 599–604.
[15] L.B. Kong, T.S. Zhang, J. Ma, F. Boey, Prog. Mater. Sci. 53 (2) (2008) 207–322.
[16] A. Castro, P. Millan, L. Pardo, B. Jimenez, J. Mater. Chem. 9 (6) (1999) 1313–1317.
[17] S.E. Lee, J.M. Xue, D.M. Wan, J. Wang, Acta Mater. 47 (9) (1999) 2633–2639.
[18] C.L. Chew, A. Srinivas, T. Sritharan, F.Y.C. Boey, Scripta Mater. 53 (10) (2005) 1197–1199.
[19] T. Hungria, H. Amorin, J. Galy, J. Ricote, M. Alguero, A. Castro, Nanotechnology 19 (15) (2008) 155609.
[20] S.Q. Hui, J. Roller, S. Yick, X. Zhang, C. ces-Petit, Y.S. Xie, R. Maric, D. Ghosh, J. Power Sources 172 (2) (2007) 493–502.
[21] E. Gomes, M.R. Soares, F.M. Figueiredo, F.M.B. Marques, J. Eur. Ceram. Soc. 25 (12) (2005) 2599–2602.
[22] V.V. Zyryanov, N.F. Uvarov, V.A. Sadykov, Y.V. Frolova, G.M. Alikina, A.I. Lukashevich, M.I. Ivanovskaya, J.M. Criado, S. Neophytides, Catal. Today 104 (2–4) (2005) 114–119.
[23] V.V. Zyryanov, V.A. Sadykov, N.F. Uvarov, G.M. Alikina, A.I. Lukashevich, S. Neophytides, J.M. Criado, Solid State Ionics 176 (37–38) (2005) 2813–2818.
[24] B.D. Cullity, in: M.A. Reading (Ed.), Elements of X-ray Diffraction. Addison-Wesley Series in Metallurgy and Materials, Addison-Wesley, Massachusetts, 1967.
[25] P. Datta, P. Majewski, F. Aldinger, J. Alloys Compd. 438 (1–2) (2007) 232–237.
[26] R.F.C. Marques, H.E. Zorel, M.S. Crespi, M. Jafelicci, C.O. Paiva-Santos, L.C. Varanda, R.H.M. Godoi, J. Therm. Anal. Calorim. 56 (1) (1999) 143–149.
[27] A. Chandrasekaran, A.M. Azad, J. Mater. Sci. 36 (19) (2001) 4745–4754.
[28] T.Y. Glavatskikh, N.U. Venskovskii, V.V. Aleksandrovskii, N.V. Golubko, A.K. Avetisov, G.M. Kaleva, A.V. Mosunov, E.D. Politova, S.Y. Stefanovich, Inorg. Mater. 39 (7) (2003) 759–763.
[29] T. Ishihara, T. Shibayama, M. Honda, H. Nishiguchi, Y. Takita, J. Electrochem. Soc. 147 (4) (2000) 1332–1337.
[30] T.Y. Chen, K.Z. Fung, J. Power Sources 132 (1–2) (2004) 1–10.
[31] M. Rozumek, P. Majewski, L. Sauter, F. Aldinger, J. Am. Ceram. Soc. 86 (11) (2003) 1940–1946.
[32] M. Alguero, J. Ricote, T. Hungria, A. Castro, Chem. Mater. 19 (2007) 4982–4990.
[33] P. Datta, P. Majewski, F. Aldinger, Mater. Chem. Phys. 102 (2–3) (2007) 240–244.
[34] H. Ishikawa, M. Enoki, T. Ishihara, T. Akiyama, J. Alloys Compd. 430 (1–2) (2007) 246–251.